American Mineralogist, Volume 98, pages 2144–2154, 2013

K-Ar dating and $\delta^{18}O$-δD characterization of nanometric illite from Ordovician K-bentonites of the Appalachians: Illitization and the Acadian-Alleghenian tectonic activity

Norbert Clauer[1,*], Anthony E. Fallick[2], Dennis D. Eberl[3], Miroslav Honty[4], Warren D. Huff[5] and Amélie Aubert[1]

[1]Laboratoire d'Hydrologie et de Géochimie de Strasbourg (CNRS-UdS), 1 rue Blessig, 67084 Strasbourg, France
[2]Scottish Universities Environmental Research Centre, East Kilbride, Glasgow G75 0QF, U.K.
[3]Emeritus, U.S. Geological Survey, 3215 Marine Street, Suite E127, Boulder, Colorado 08303, U.S.A.
[4]SCK-CEN, Health, Environment and Safety Institute, Boeretang 200, 2400 Mol, Belgium
[5]Department of Geology, University of Cincinnati, Cincinnati, Ohio 45221-0013, U.S.A.

Abstract

Nanometric (<0.02, 0.02–0.05, 0.05–0.1, 0.1–0.2 μm) illite fractions were separated from K-bentonite samples from northwestern Georgia, and studied by X-ray diffraction, oxygen and hydrogen isotope geochemistry, and K-Ar dated to more tightly constrain the tectono-thermal history of the Appalachian orogeny. Their XRD patterns are very similar for a given sample with respect to the peak shapes and positions. They are ordered illite-smectite mixed layers with only small variations in the relative proportions of illite and smectite interlayers. The illite crystal thickness distributions also are very homogeneous across the various size fractions of the same sample, but crystallite thickness varies from sample to sample. It can be concluded from the α-β^2 diagram that illitization occurred in all fractions by simultaneous nucleation and crystal growth, except for one sample. In that sample, a period of growth without nucleation was detected on top of the nucleation and growth episode.

The K-Ar ages organize into two isochrons, the first at 319.9 ± 2.0 Ma with an initial $^{40}Ar/^{36}Ar$ ratio of 271 ± 66 Ma, and the second at 284.9 ± 1.2 Ma with an initial $^{40}Ar/^{36}Ar$ ratio of 310 ± 44. One data point above the older isochron and three between the two isochrons suggest a detrital contamination for the former separate and a possible further generation of nanoparticles for the three others. The samples with the older crystallization age consist of illite and illite-rich mixed-layers, and those with the younger age contain smectite-rich mixed-layers without illite, or illite-enriched illite-smectite mixed-layers. The K-Ar ages fit the age trends published previously for similar K-bentonites with regional age patterns between 240 and 270 Ma in the southwestern region, between 270 and 300 Ma in the central zone and the southern Appalachians, and between 315 and 370 Ma in the northernmost.

Each of the two generations of illite crystals yields very consistent $\delta^{18}O$ (V-SMOW) values at 17 ± 1‰ for the older and at 21 ± 1‰ for the younger. If crystallization temperatures of the nanometric illite were between 100 and 200 °C, as suggested by microthermometric determinations, the hydrothermal fluids had $\delta^{18}O$ values of 4 ± 1‰ in the Dalton district and of 8 ± 1‰ in the Lafayette, Trenton, and Dirtseller districts at 100 °C, and of 11 ± 1 and 15 ± 1‰ in the same locations at 200 °C, probably because the water-rock isotope exchanges at elevated temperature occurred in rock-dominated systems. The $\delta^{18}O$ of the fluids remained unchanged during local crystal growth, but varied depending on the geographic location of the samples and timing of illitization. The δD (V-SMOW) values of the different size fractions do not provide consistent information; they range from –70 to –45‰ for most nanometric and micrometric fractions (V-SMOW), but with no apparent coherent pattern.

Nanometric illite-rich crystals from K-bentonite that underwent tectono-thermal alteration yield constant ages, constant clay mineralogy, constant crystallite size distributions for all of the nucleating and growing illite-type crystals of each sample, as well as constant $\delta^{18}O$ values implying constant fluid chemistry, all pointing to geologically sudden crystallization.

Keywords: Nanometric "fundamental" particles, XRD mineralogy, K-Ar dating, $\delta^{18}O$ and δD geochemistry, Ordovician K-bentonites, U.S. midcontinent, Acadian/Alleghenian orogeny

Introduction

The outcrop area of Ordovician K-bentonites from the U.S. midcontinent extends between Oklahoma to the southwest, Ontario to the northeast and Tennessee to the south with additional outcrops further to the southeast in Georgia and Alabama (Kolata et al. 1996; Leslie et al. 2008). The area is conventionally divided into several intracratonic basins and arches, including the foreland basins of the Appalachian and Ouachita orogens, once filled with thick sequences of Pennsylvanian and Permian sediments derived from the Alleghenian Orogeny (Beaumont et al. 1987). The Ordovician K-bentonites belong to a platform sedimentary sequence, where they are hosted by limestones overlain by a

* E-mail: nclauer@unistra.fr

thick shale sequence resting on thick sandstone beds of Cambrian and Ordovician age and deposited on the Precambrian basement (e.g., Grathoff et al. 2001). Illitization of smectite from these K-bentonites was examined by Elliott and Aronson (1993) who reported a tendency toward a more smectitic composition with increasing distance from the orogenic front, the overall illite-smectite composition being locally quite homogeneous, even in the westernmost parts of the area (Hay et al. 1988). Lower smectite-layer occurrences in the clay material (<15%S) were recorded in the folded zone of the orogeny in the Appalachian Basin (Elliott and Haynes 2002). No compositional change was reported between the foreland basin that may have experienced up to 3 km of Upper Paleozoic cover and the inter-cratonic areas where such cover was minimal (Beaumont et al. 1987). Numerous occurrences of authigenic K-feldspar were also documented in the bentonite beds of the western part of the area (Hay et al. 1988), as well as in the carbonate beds underlying the bentonite units of the Appalachian Basin (Hearn et al. 1987). An intense development of K-feldspar along with filamentous illite has also been documented below the bentonite beds over the whole cratonic area, in the St. Peter and Mt. Simon thick sandstone beds and in the regolith at the contact with the crystalline basement (Woodard 1972; Marshall et al. 1986; Harper et al. 1995; Duffin et al. 1989; Ziegler and Longstaffe 2000a; Chen et al. 2001; Liu et al. 2003).

The K-bentonite units containing well-crystallized illite-rich clay material are, therefore, interesting units to be isotopically dated for complementary reconstruction of the tectono-thermal activity of this midcontinental area. Available K-Ar data on illite-smectite from K-bentonites outline a clear regional pattern with younger ages between 240 and 270 Ma in the southwestern zone, intermediate ages between 270 and 300 Ma in the central zone and in the southern Appalachians, and older ages from 315 to 370 Ma toward the north (Elliott and Aronson 1987, 1993; Hay et al. 1988). Similar ages were recorded also for filamentous illite in the underlying sandstones (321–366 Ma; Girard and Barnes 1995; Ziegler and Longstaffe 2000b) and in the regolith (294–342 Ma; Ziegler and Longstaffe 2000a) to the north. This geographic distribution of K-Ar data parallels the tectonic events in the neighboring orogenic belt characterized by the late Devonian Acadian phase to the north and the Carboniferous-Permian Alleghenian phase in the more central and southern parts of the area.

The K-feldspar described in the Cambrian carbonate rocks and the illite-smectite of the Ordovician K-bentonites are contemporaneous in the southern Appalachian Basin, where fluid inclusions in the feldspar grains indicate a temperature range of 100–200 °C and a salinity of 18–21% NaCl equivalent for the interacting brines (Hearn et al. 1987; Elliott and Haynes 2002). Paleotemperatures well above 100 °C were also reported, both in the southern Appalachian Basin and the nearby foreland area (7–27% smectite layers in the illite-smectite mixed layer), on the basis of reset apatite fission tracks and partially reset zircon fission tracks (Roden et al. 1993). Long-distance migration of hot saline fluids has been invoked to explain these observations (Hearn et al. 1987; Elliott and Haynes 2002).

In the western midcontinent, the K-feldspars of the bentonite beds give clearly older K-Ar ages than the illite-smectite mixed layers (375–400 Ma; Hay et al. 1988). Similar or even older ages were obtained for K-feldspars from underlying rocks (Woodard 1972; Marshall et al. 1986; Duffin et al. 1989; Ziegler and Longstaffe 2000a; Chen et al. 2001; Liu et al. 2003). The petrographic evidence from sandstones indicates that K-feldspar and quartz crystallized at the same time, after the first generation illite-smectite, but before the second-generation illite-smectite (Fishman 1997). Fluid flow events of different nature are hypothesized to explain these observations.

Toulkeridis et al. (1998) dated biotite and clay separates of Ordovician K-bentonite units sampled in Alabama and Tennessee by the K-Ar, Sm-Nd, and Rb-Sr methods. The biotite K-Ar ages at 459 ± 10 Ma were consistent with a Late-Ordovician deposition age for the bentonites. The clay fractions leached with dilute HCl provided a Sm-Nd isochron for the clay residues of 397 ± 44 Ma indicative of a crystallization during Acadian tectono-thermal activity at about 200 °C, and a distinct younger Sm-Nd isochron of 285 ± 18 Ma for the acid leachates that represent distinct soluble mineral phases intimately associated with the clay particles. The Sm-Nd age of these non-silicate mineral phases is close to the K-Ar ages obtained previously on the clays in other areas of the eastern midcontinent, suggesting a thermally induced recrystallization of the clay material but also of associated soluble minerals during the Alleghenian-Ouachita orogenic activity. The Rb-Sr system of the clay material was variably disturbed, except for the sample taken near the Allegheny Front for which an age of 179 ± 4 Ma suggests further tectono-thermal activity.

The age summary indicates that the tectonic and thermal history of the southern North American midcontinent is complex. The region experienced a thermal event of Acadian age recorded by the data of K-feldspars, and a further overprint by an Alleghenian thermal episode, which advanced the degree of the original illitization. It can therefore be considered that at least some of the available data generated from illite-smectite material represent mixing of illite contributions from the two events. Our attempt here to provide new information is based on the study of illite "fundamental" nanometric particles separated from illite-smectite mixed layers (labeled I/S hereafter) of K-bentonite units purposely collected close to the Alleghenian Front in Tennessee, together with one reference sample taken away from the front in Alabama, to: (1) date them with the K-Ar method to constrain tectonic/hydrothermal regional episodes independent of the already available regional age cover, and (2) characterize the $\delta^{18}O$ and δD compositions of these nanometric crystals for new information on the oxygen and hydrogen isotope composition of the fluids that interacted with the nucleating and growing crystals and on the crystallization conditions of the illite crystals, to understand more about initial illitization in these volcanic materials.

The rationale for separating and analyzing nanometric I/S is that they normally consist of non-swelling coherent illite domains that are enriched in K and of smectite-type interlayers that are actually the shared expandable interfaces between adjacent illite crystals. Basically, the smaller the illite domains, the larger is the proportion of swelling interlayers that occur in the I/S structure. The illite crystals of such I/S were named "fundamental particles" by Nadeau et al. (1984) who were the first investigators to separate and examine these individual illite crystals. Their dispersion by infinite osmotic swelling allows

"cleaning" of the swelling smectite-type interlayers that then become smectite-reacting surfaces of illite crystals, while the illite interlayers remain collapsed. As the term "fundamental" may be ambiguous to readers not fully familiar with these specific crystallographic studies, we have identified these crystals hereafter as "nanometric" relative to coarser separates, only referring to one-dimension of their size. The smectite-reacting surfaces of the illite crystals are termed smectite sites according to terminology used by Altaner and Ylagan (1997).

Geologic setting and sample description

Numerous K-bentonite beds have been described in the Ordovician carbonate rock-dominated sedimentary sequence of the eastern United States (Huff et al. 1986; Huff and Kolata 1990). They consist mainly of I/S resulting from alteration of felsic volcanic ash that induced progressive transformation of the initial smectite into illite. Isotopic support for basin-wide migration of hot saline fluids during this orogeny (Elliott and Aronson 1987, 1993) was also documented by $^{40}Ar/^{39}Ar$ ages between 278 and 322 Ma for authigenic K-feldspar crystals from Cambrian limestones throughout the central Appalachian basin (Hearn and Sutter 1985; Hearn et al. 1987). Remagnetization ages of ca. 255 and 275 Ma were also reported across the central Appalachians related to folding and thrusting (Stamatakos et al. 1996). These results provided new insights into the debate about movement of hot saline fluids through sedimentary basins (Dozy 1970; Garven and Freeze 1984; Bethke 1986; Oliver 1986; Bethke and Marshak 1990), knowledge of which is essential to elucidate how the K-bentonites evolved after deposition. The fact that the isotopic ages varied by up to 30–40 million years made it difficult to postulate a single continuous illitization process over this extended period of time. The present study was designed to refine and investigate in detail this age span, and also to identify specific regional events that have occurred during the entire Alleghenian-Acadian orogeny by analyzing smaller illite-rich size fractions than have been previously studied. The Middle-Upper Ordovician succession in the Allegheny Front is divided into a dominantly carbonate western facies and a largely siliciclastic eastern facies separated by the Helena thrust fault. Stratigraphic and sedimentologic descriptions are available in Drahovzal and Neathery (1971, 1985), Raymond et al. (1988), and Szabo et al. (1988).

Nine samples were collected in northwestern Georgia at the boundary with Tennessee to the North and Alabama to the West (Fig. 1). They were taken close to the Allegheny Front, in an area delimited by the cities of Dalton, Lafayette, and Trenton. Samples 1A and 1B are from Hamilton Mountain near Dalton, appearing in strata broken by small faults that belong to the 83 m thick Greensport Formation, which is composed of a lower unit of reddish gray, shaly, micritic limestone, a middle unit of red shale, and an upper unit of interbedded red shale and sandstone (Carter and Chowns 1989). The two samples represent, respectively the base and the top of a 53 cm thick K-bentonite unit probably corresponding to the T3 Deicke bentonite of the Tennessee section. The 1A lower bed contains some thin interlayered red-shale beds, which could have resulted from some reworking during and immediately after deposition. The three samples 2A, 2B, and 2C also coming from near Dalton represent the base, middle and top of a 60 cm thick K-bentonite bed probably corresponding to the T4 Millbrig K-bentonite of the Tennessee section. Sample 3A was taken about 8 miles NW of Lafayette, Georgia, near Davis Crossroads in the 15–30 m thick Carters Limestone, which is part of the Middle Ordovician Stones River Group in eastern Tennessee, and consists of fine-grained, yellowish-brown limestone, slightly cherty with several thin bentonite beds. Sample 3B is located S of Trenton in a 1 m thick unit interbedded with carbonate with some silicification. Sample 4A is the only one collected outside of Georgia; it comes from the Dirtseller Mountain quarry in Alabama and belongs to the Millbrig K-bentonite. Sample 4B belongs also to the Millbrig K-bentonite, but near Dalton, Georgia. A more detailed stratigraphic positioning, especially for the Deicke and Millbrig samples, can be found in Kolata et al. (1996).

Figure 1. Geographic location of the sampling sites. From north to south, sample 3B was collected near Trenton, samples 1A, 1B, 2A, 2B, 2C, and 4B come from near Dalton, sample 3A was taken near Lafayette, and sample 4A at Dirtseller Mountain.

Analytical procedure

Whole-rock samples were crushed, sieved to 0.16 mm, and dropped into deionized water to be disaggregated using an ultrasonic bath. The <2 µm size fraction of each slurry was separated by sedimentation after treatment with sodium acetate, hydrogen peroxide and sodium dithionite according to the procedure of Jackson (1975). Recovered by high-speed ultracentrifugation, the <0.2 µm size fraction was further divided into four nanometric sub-fractions (<0.02, 0.02–0.05, 0.05–0.1, and 0.1–0.2 µm) by continuous-flow high-speed ultracentrifugation after infinite swelling, following Środoń et al. (1992). A combined chemical treatment and infinite swelling are applied to micrometric I/S to separate the non-swelling coherent illite domains with K-rich interlayers from smectite domains with K-depleted interlayers. The consequence is that the smectite-rich domains in the nanometric size fractions identified as such by XRD are most probably the shared expandable (swelling) interfaces between adjacent illite crystals. The excess soluble salts were removed by centrifugation and dialysis. X-ray diffraction (XRD) patterns were made on oriented air-dried (AD) and ethylene-glycolated (EG) specimens using a Siemens D500 XRD system with a graphite monochromator, Cu$K\alpha$ radiation, a range of 2–32° 2θ, a step size of 0.02° 2θ and 5 s per step count time. The expandability (called $\%S_{XRD}$) was determined using a modified version of the δ two-θ method of Moore and Reynolds (1997) on the glycolated specimens

$$\%S_{XRD} = 466.4 - 96.9\Delta + 5.0\Delta^2$$

where Δ represents the difference in two θ between the I/S peak at about 17° and the two-θ value for the peak at about 9°. This equation was derived from NEWMOD calculations.

The mean thickness and thickness distribution of the nanometric illite crystals were determined for the separated fine and ultrafine fractions by XRD after

PVP-10 intercalation into the expandable interlayers to remove the cations held in the smectite-type interlayers and therefore improve subsequent X-ray diffraction analysis and measurement of crystallite size distributions (Eberl and Środoń 1988; Dudek and Środoń 1996; Eberl et al. 1998a). Fundamental illite crystal thickness distribution (CTD) was determined from first-order reflections using the Bertaut-Warren-Averbach (BWA) method (Drits et al. 1998) and the MudMaster program (Eberl et al. 1996). This method gives accurate measurements of mean thicknesses only for I/S particles that consist of <50% smectite layers, because the method is not able to detect smectite monolayers that potentially occur in more highly smectitic clays. Crystal-growth mechanisms that reproduce the measured CTDs of the different size fractions were simulated using the GALOPER program (Eberl et al. 2001). The volume-weighted and area-weighted mean thicknesses were calculated according to the BWA theory, and the parameters α (= mean of the natural logarithms of the thicknesses) and β^2 (= variance of the natural logarithms of the thicknesses) parameters were calculated from CTDs. These α and β^2 parameters of the different size fractions were plotted in a diagram along with other previously obtained results to evaluate the crystal growth reaction paths according to theory of Eberl et al. (1998b), in the manner of Bove et al. (2002).

The K-Ar determinations were made using a procedure similar to that of Bonhomme et al. (1975). Potassium was measured by flame spectrophotometry with an accuracy of 1.0%. For Ar analyses, the samples were preheated under vacuum at 80 °C for at least 12 h to reduce the amount of atmospheric Ar adsorbed on the mineral surfaces during sample preparation, separation and handling. The results were controlled by repetitive analysis of the GL-O glauconite standard, which averaged $24.57 \pm 0.11 \times 10^{-6}$ cm^3/g STP (2σ) of radiogenic ^{40}Ar for 5 independent determinations made during the course of the study. The $^{40}Ar/^{36}Ar$ ratio of the atmospheric Ar was also measured periodically, averaging 298.5 ± 1.0 (2σ) during the same period for 4 independent determinations. The recommended values being $24.85 \pm 0.24 \times 10^{-6}$ cm^3/g for the amount of radiogenic ^{40}Ar in the glauconite standard (Odin et al. 1982), and 295.5 for the atmospheric $^{40}Ar/^{36}Ar$ ratio (Nier 1950), the measured values were considered to be internally consistent with small uncertainties and close enough to the theoretical values not to require discrimination corrections to the individual determinations. The gas volume of the blank of the extraction line and the mass spectrometer was also determined before each Ar extraction. Systematically in the 10^{-8} cm^3 range, which is far below the contents of the different size fractions, the ^{40}Ar blank content was disregarded in the age calculations. The usual decay constants were used for the age calculations (Steiger and Jäger 1977), and the overall error is evaluated to be routinely better than 2% (2σ).

For the hydrogen isotope analyses, the samples were first vacuum-degassed at 200 °C overnight to remove the interlayer and absorbed surface water and were then transferred to a previously out-gassed Pt crucible. The crucible was placed inside a quartz extraction chamber, which was then attached to the vacuum line and evacuated. Dehydroxylation was accomplished by radiofrequency induction heating of the crucible at 1200 °C. The released water was converted to H_2 by reaction with Cr at 800 °C (Bigeleisen et al. 1952; Donnelly et al. 2000) in a multiple-pass system. The H_2 yield was measured manometrically and δD determined on a gas-source mass spectrometer calibrated via water and mineral standards. With this analytical technique, the NBS30 biotite standard gave a δD of –65‰ (V-SMOW) and an analytical precision of ±6‰ (2σ) (see Fallick et al. 1993); this value represents the long-term reproducibility achieved by multiple analysts for an in-house kaolinite standard. The oxygen isotope composition of the clay minerals was determined by laser fluorination (Macaulay et al. 2000) based on the Borthwick and Harmon (1982) BrF_5 modification to the method of Clayton and Mayeda (1963). The long-term precision was ±0.6‰ (2σ) for an in-house quartz standard analyzed by multiple analysts, and the NBS28 quartz standard yielded an $\delta^{18}O$ of 9.6‰ (V-SMOW). All clay isotope data are reported in per mil (‰) relative to the V-SMOW standard. As indicated in a later table, two duplicates of $\delta^{18}O$ values report internal reproducibility of ±0.6 to ±0.9% among the determinations. The stable isotope data reported here were all determined by one analyst over a short time interval; we propose that it is why the inter-sample consistency (see next section: Results) appears better than the long-term, multi-analyst technique precision quoted for $\delta^{18}O$; there was insufficient sample material to allow δD replicate analyses.

Results

XRD data

For any given sample, the XRD patterns of the air-dried nanometric size fractions are very similar with respect to the peak shapes and positions. They indicate that the size fractions contain ordered I/S of R3 Reichweite, which represents another way to quantify ordering of the I/S from disorder R0 type to highly ordered R3 type, with smectite-layer contents ranging from 6 to 23% (Moore and Reynolds 1997). Generally, the smectite-layer content does not change significantly with size fraction for a given sample, and kaolinite was detected in minute amounts in a few size fractions (Table 1). Examples of XRD patterns for air-dried and glycol-solvated sample 4A are given in Figures 2a and 2b. Swelling was removed by PVP intercalation, and the resulting XRD patterns for the 001 peaks, shown for sample 4A in Figure 3, were analyzed by MudMaster program to yield mean crystallite thicknesses (Table 1) and crystallite thickness distributions, examples of which are given for sample 4A in Figure 4. The particle thickness distribution patterns are systematically very homogeneous for the different size fractions of the studied samples (Fig. 4), which is consistent with, but does not imply that the coarser size fractions comprise aggregates of smaller particles.

To check the accuracy of the MudMaster-determined crystallite thickness distributions, the XRD pattern for glycolated sample 4A was back-calculated from crystallite thickness fre-

Table 1. XRD results on the studied size fractions

Samples	Size (μm)	Smectite layers (%)	Kaolinite	Mean crystallite thickness (nm) Area weighted	Volume weighted
1A = base of Deicke Formation (T3 bentonite unit) at Dalton, Georgia					
1A1	<0.02	11	N	3.7	4.9
1A2	0.02–0.05	11	N	4.0	5.4
1A3	0.05–0.1	12	Y	4.2	6.0
1A4	0.1–0.2	10	Y	4.2	6.4
1B = top of the unit					
1B2	0.02–0.05	8	Y	3.7	5.0
1B3	0.05–0.1	7	Y	4.1	6.1
1B4	0.1–0.2	6	Y	4.0	6.3
2A = base of Deicke Formation (T3 bentonite unit) at Dalton, Georgia					
2A1	<0.02	19	N	3.8	5.4
2A2	0.02–0.05	18	N	3.8	5.0
2A3	0.05–0.1	19	N	3.6	4.9
2A4	0.1–0.2	22	N	3.4	4.5
2B = middle of the unit					
2B1	<0.02	17	N	3.3	4.3
2B2	0.02–0.05	20	Y	3.3	4.3
2B3	0.05–0.1	20	Y	3.3	4.2
2B4	0.1–0.2	20	Y	3.1	3.9
2C = top of the unit					
2C1	<0.02	13	N	3.0	3.9
2C2	0.02–0.05	13	Y	3.2	4.3
2C3	0.05–0.1	18	Y	3.1	4.2
2C4	0.1–0.2	18	Y	3.3	4.4
4B = Millbrig Formation at Dalton, Georgia					
4B1	<0.02	18	N	3.2	4.1
4B2	0.02–0.05	18	N	3.2	4.3
4B4	0.1–0.2	21	N	3.1	4.2
3A = Deicke Formation of Lafayette, Georgia					
3A1	<0.02	22	N	3.5	4.5
3A2	0.02–0.05	22	N	3.5	4.5
3A3	0.05–0.1	22	N	3.4	4.5
3A4	0.1–0.2	23	N	3.3	4.4
3B = South of Trenton, Georgia					
3B1	<0.02	15	N	3.5	4.4
3B2	0.02–0.05	14	N	3.7	4.5
3B3	0.05–0.1	16	N	3.7	4.6
3B4	0.1–0.2	17	N	3.5	4.2
4A = Millbrig Formation at Dirtseller, Alabama					
4A1	<0.02	13	N	3.4	4.9
4A2	0.02–0.05	12	N	3.5	4.8
4A3	0.05–0.1	12	N	3.6	5.0
4A4	0.1–0.2	13	N	3.6	4.6

Note: N stands for no and Y for yes.

quencies using the StackMan program (Eberl et al. 2011). This calculation assumes that I/S forms by the random stacking of illite crystals having different thicknesses. Smectite layers at the interfaces between crystals are considered to result from water and glycol adsorbed on crystal surfaces. For this calculation, it was assumed that each of the stacks (MacEwan crystallites) contains two illite crystals and, therefore, one smectite interlayer per stack. The frequency distribution determined by MudMaster program for sample 4A is given in Figure 5, as is the StackMan pattern that was calculated from these frequencies. The correspondence between calculated and measured patterns is excellent in peak intensity and location, thereby indicating that the thickness frequency distributions that were determined are accurate. The α-β^2 diagram confirms that, except for sample 3B, illitization occurred in all size fractions by the mechanism of simultaneous nucleation and growth, probably along a closed-system pathway that is expected for compacted bentonite beds (Fig. 6). The fractions of sample 3B that plot off this curve represent a growth mechanism that initially underwent a period of simultaneous nucleation and growth, followed by growth only (Bove et al. 2002). These fractions yield also the youngest K-Ar ages and could have crystallized in a geochemical system characterized by a higher degree of fluid circulation, explaining the two successive growth mechanisms.

A plot of volume or area-weighted mean crystallite thickness relative to the K-Ar age suggests no relation that is mathematically convincing between mean particle thickness and age (Fig. 7). However, it might be argued that the three fractions that have older individual ages at about 320 Ma appear to be slightly thicker (at 6 nm). This increase in the particle thickness of the older fractions could result from slightly more intense illitization. Also noteworthy are the values of the water yields obtained in measuring the stable isotope compositions (Table 2): the narrow range, mostly from 2.7 to 3.3 µmol/mg, also suggests a very homogeneous particle composition of the size fractions.

TABLE 2. $\delta^{18}O$ and δD values for the studied size fractions

Samples	Size (mm)	Yields (mmol/mg)	$\delta^{18}O$ (V-SMOW)	δD (V-SMOW)
1A = base of T3 bentonite unit at Dalton, Georgia				
1A1	<0.02	2.2	17.4	–26
1A2	0.02–0.05	3.1	17.9	–70
1A3	0.05–0.1	3.1	17.0	–47
1B = top of the unit				
1B2	0.05–0.1	4.1	17.7	–41
1B4	0.1–0.2	4.2	17.5	–54
2A = base of T3 bentonite unit at Dalton, Georgia				
2A1	<0.02	3.4	16.4	–90
2A2	0.02–0.05	3.2	16.6	–71
2A3	0.05–0.1	2.7	16.5	–64
2B = middle of the unit				
2B1	<0.02	3.1	16.5	–61
2B2	0.02–0.05	2.9	15.8	–62
2B3	0.05–0.1	2.8	16.0	–64
2C = top of the unit				
2C1	<0.02	3.3	16.8	–68
2C2	0.02–0.05	3.1	16.3	–60
2C3	0.05–0.1	3.0	16.3	–57
3A = Deicke Formation of Lafayette, Georgia				
3A2	0.02–0.05	3.1	20.5	–55
3A3	0.05–0.1	3.0	20.6	–48
3A4	0.1–0.2	2.7	20.6	–53
3B = South of Trenton, Georgia				
3B1	<0.02	3.3	21.6	–50
3B2	0.02–0.05	2.7	22.2	–69
3B3	0.05–0.1	2.7	21.5	–67
4A = Millbrig Formation at Dirtseller, Alabama				
4A1	<0.02	3.3	21.8	–68
4A2	0.02–0.05	2.9	21.6	–47
4A3	0.05–0.1	2.9	21.7	–50
4B = Millbrig Formation at Dalton, Georgia				
4B1	<0.02	3.3	17.0	–70
duplicate			16.8	
4B2	0.02–0.05	2.7	16.5	–68
duplicate			16.2	

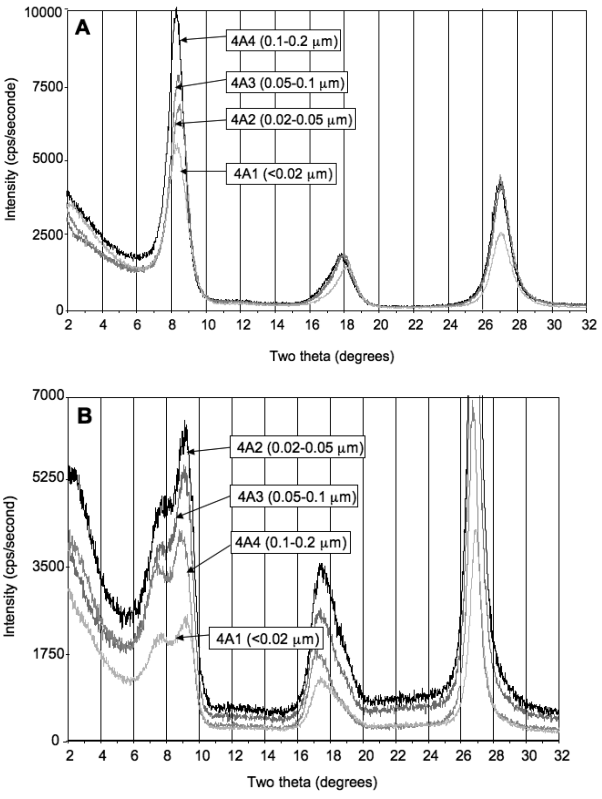

FIGURE 2. XRD patterns of the air-dried (**a**) and ethylene-glycolated (**b**) size fractions of sample 4A.

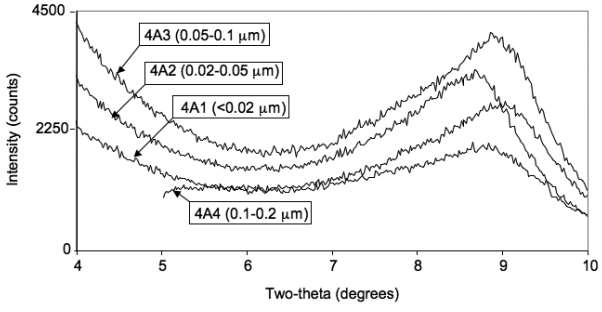

FIGURE 3. XRD patterns of the polymer PVP-treated size fractions of sample 4A.

$\delta^{18}O$ data

Twenty-five nanometric size fractions were analyzed for $\delta^{18}O$, which ranges from 15.8 to 22.2‰ (V-SMOW). Determination of the δD also provided precise measurements (±10%) of the H_2O^+

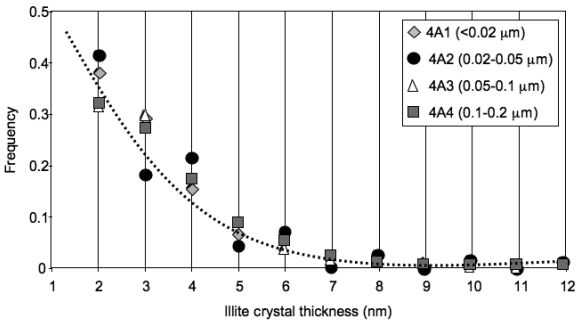

FIGURE 4. Measured vs. calculated XRD pattern of a size fraction from sample 4A.

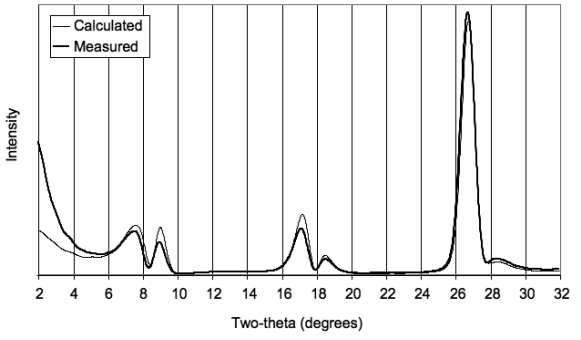

FIGURE 5. Measured vs. StackMan-calculated XRD pattern of the glycolated 0.1–0.2 mm size fraction from the sample 4A. The pattern was calculated from the crystallite size distribution and the 2:1 layer parameters found in Eberl et al. (2011), using a variable Lp factor with an orientation function (σ*) of 2.3.

content of the fractions (Table 2). The yields are scattered for the different size fractions of the same sample, with water contents of the coarser fractions either lower (samples 1A and 3A) or higher (samples 2A and 2C) than those of the two intermediate grain sizes. These variations do not clearly correspond either to the amounts of smectite-type swelling layers in the I/S structures (Table 1) or to variations of their $\delta^{18}O$.

The other notable analytical observation is that the nanometric size fractions of each sample have internally very consistent $\delta^{18}O$; the 2σ analytical dispersion never exceeds ±0.4‰ for each set of values (see comment above in the Analytical Procedure section about dispersion). The $\delta^{18}O$ values for the 18 size fractions from the 6 samples of the Dalton district range very narrowly from 15.8 ± 0.4‰ for sample 2B to 17.9 ± 0.1‰ for sample 1A (Table 2), whereas those from samples collected at Lafayette, Trenton and Dirtseller Mountain have systematically higher and also narrowly spread $\delta^{18}O$ values from 20.5 ± 0.1 to 22.2 ± 0.3‰.

δD data

The same 25 size fractions were also analyzed for δD; the values ranging widely from –90 to –26‰ (V-SMOW), although the spread is reasonably narrow for most size fractions of individual samples, apart from 1A and 2A samples (from –26 to –70‰ and from –64 to –90‰, respectively). The δD of the three size fractions of samples 2B, 3B, and 4B vary very narrowly,

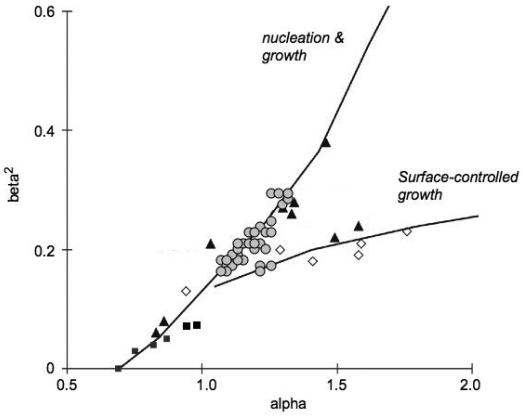

FIGURE 6. Alpha-beta^2 diagram for the different nanometric size fractions of the studied samples. Most data points (gray circles) plot near the nucleation + growth curve. Only three fractions plot away on the surface-controlled curve. The black triangles represent hydrothermal bentonites from another study (Eberl et al. 1998b) and the black rectangles represent diagenetic illite/smectite mixed-layers from East Slovak Basin (Sucha, unpublished data).

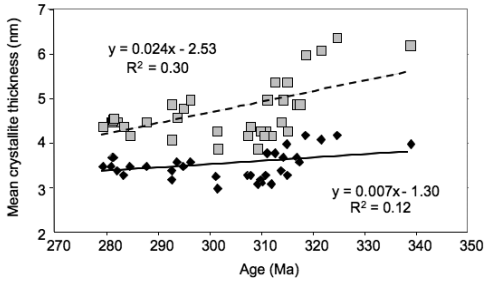

FIGURE 7. Mean thickness in nm, by area (the black diamonds) and volume (the gray squares) weight, relative to the K-Ar ages of the different nanometric size fractions.

whereas two of the three δD are close and the third quite distinct for samples 3A, 4A, and 2C. In summary, there is no clear pattern apparent in the δD values, except that the δD values are equivalently narrowly scattered as the $\delta^{18}O$ values in some cases.

K-Ar data

The K-Ar ages of the different nanometric size fractions of each sample are almost identical throughout the suite of results (Table 3), significantly below the usual individual analytical uncertainty. Only the coarsest analyzed size fraction of sample 1B is significantly older than all other fractions. Such a distinct age is very rare in K-bentonite units, especially in their nanometric fundamental particles (e.g., Clauer et al. 1997; Środoń and Clauer 2001; Środoń et al. 2006). The discrepancy for sample 1B most probably reflects a bias introduced by the addition of some detrital material from the overlying or underlying sedimentary unit during or after deposition, which although rare can occur due to some syn- or post-depositional reworking. This explanation is supported here by the occurrence of thin interbeds of red shale in the K-bentonite unit.

The data range narrowly within 2 Ma for the size fractions of samples 4A and 3B, within 3 Ma for those of samples 3A, 2B, 2A, and 1B, within 5 Ma for those of samples 1A and 2C after discarding the age of the coarsest fraction, and within 6 Ma for those of sample 4B. Also, the K-Ar ages are very similar for the nanometric fractions at the base and top of the same K-bentonite beds. For instance, the average values of the size fractions from samples 1A and 1B are within 1 Ma, and the base and intermediate layers of samples 2A and 2B are within 3 Ma, whereas the top sample 2C appears to have reacted longer (or later) by 10 to 14 Ma.

The entire set of K-Ar ages ranges from 279 ± 7 to 324 ± 8 Ma, which is similar to those available in the literature from the same area (Hearn and Sutter 1985; Hearn et al. 1987; Elliott and Aronson 1987, 1993; Hay et al. 1988). However, a detailed look at the results shows four tightly grouped average ages at 279–281 Ma for samples 3A and 3B, 304–305 Ma for samples 2C and 4B, 310–312 Ma for the samples 2A and 2B, and 317–318 for the samples 1A and 1B. Only the sample collected away from the Allegheny Front provides a set of K-Ar ages that is in between the two young age averages at about 293 ± 2 Ma.

TABLE 3. K-Ar data of the studied size fractions

Samples	Size (μm)	K_2O (%)	Ar* (%)	$^{40}Ar^*$ (10^{-6} cm^3/g)	$^{40}Ar/^{36}Ar$ (10^{-3})	$^{40}K/^{36}Ar$ (10^{-6})	Age (Ma ± 2δ)	Avg.
1A = base of T3 bentonite unit at Dalton, Georgia								
1A1	<0.02	4.69	88.85	52.31	2650	116	316.6 (7.7)	318
1A2	0.02–0.05	4.90	91.19	54.30	3353	151	314.7 (7.5)	+
1A3	0.05–0.1	5.51	90.78	61.82	3204	142	318.3 (7.5)	–
1A4	0.1–0.2	5.43	91.53	62.20	3490	153	324.4 (7.6)	5
1B = top of the unit								
1B2	0.02–0.05	4.79	91.69	52.94	3558	161	314.0 (7.4)	317
1B3	0.05–0.1	4.68	90.21	53.06	3017	132	321.4 (7.7)	+
1B4	0.1–0.2	4.35	91.95	52.21	3672	154	338.6 (8.1)	3
2A = base of T3 bentonite unit at Dalton, Georgia								
2A1	<0.02	6.05	88.47	66.49	2562	113	312.4 (7.4)	312
2A2	0.02–0.05	6.13	92.96	67.03	4196	195	310.9 (7.1)	+
2A3	0.05–0.1	6.06	90.06	67.73	2974	131	317.2 (7.4)	–
2A4	0.1–0.2	6.16	89.39	67.98	2785	124	313.6 (7.4)	3
2B = middle of the unit								
2B1	<0.02	5.64	90.96	62.52	3267	147	314.8 (7.4)	310
2B2	0.02–0.05	5.96	90.87	64.97	3237	148	310.0 (7.2)	
	0.02–0.05 dupl.	5.92	89.85	64.65	2911	131	310.6 (7.3)	+
2B3	0.05–0.1	6.11	87.05	65.92	2282	91	307.1 (7.4)	–
2B4	0.1–0.2	6.12	87.45	66.49	2354	104	309.1 (7.4)	3
2C = top of the unit								
2C1	<0.02	5.15	87.90	54.42	2443	113	301.3 (7.3)	305
2C2	0.02–0.05	5.56	90.72	58.74	3184	149	301.2 (7.1)	+
2C3	0.05–0.1	5.59	88.32	61.30	2531	116	311.7 (7.5)	–
2C4	0.1–0.2	5.66	88.52	61.18	2574	117	307.7 (7.4)	5
3A = Deicke Formation of Lafayette, Georgia								
3A1	<0.02	5.89	84.49	57.64	1905	91	280.7 (7.0)	283
3A2	0.02–0.05	6.01	90.28	60.38	3040	150	287.5 (6.7)	+
3A3	0.05–0.1	6.31	88.63	62.02	2599	129	281.8 (6.7)	–
3A4	0.1–0.2	6.30	88.66	62.20	2606	128	283.0 (6.7)	3
3B = South of Trenton, Georgia								
3B1	<0.02	6.33	90.28	61.58	3040	155	279.1 (6.5)	281
3B2	0.02–0.05	6.56	92.45	64.23	3912	202	280.8 (6.4)	+
3B3	0.05–0.1	6.63	93.30	64.98	4409	229	281.1 (6.3)	–
3B4	0.1–0.2	6.56	93.08	65.09	4270	218	284.3 (6.4)	2
4A = Millbrig Formation at Dirtseller Mountain, Alabama								
4A1	<0.02	5.95	93.97	60.85	4262	215	292.4 (6.1)	293
4A2	0.02–0.05	6.17	93.07	60.20	3770	199	294.6 (6.7)	+
4A3	0.05–0.1	6.31	91.90	65.40	1960	91	296.0 (6.3)	–
4A4	0.1–0.2	6.28	93.15	64.49	4315	223	293.4 (6.7)	2
4B = Millbrig Formation at Dalton, Georgia								
4B1	<0.02	5.09	85.01	52.07	1971	90	292.4 (7.6)	304
4B2	0.02–0.05	5.41	90.98	58.89	3275	150	309.6 (7.3)	+
4B4	0.1–0.2	5.66	90.14	61.73	2997	136	310.2 (7.3)	6

Notwithstanding the fact that the number of studied samples is limited, it is interesting that each "step" in age has been recorded in all nanometric size fractions of two distinct samples having very similar mineral compositions and $\delta^{18}O$ values. This suggests that the distinct steps could have geological meaning especially since the age data do not overlap.

A plot of the $^{40}Ar/^{36}Ar$ vs. $^{40}K/^{36}Ar$ yields two straight lines, and four data points lying off these lines: three between the two lines and one above the upper of the two lines (Fig. 8). The characteristics of the two lines respectively correspond to an age of 319.9 ± 2.0 Ma for the upper line with an initial $^{40}Ar/^{36}Ar$ ratio of 271 ± 66, and 284.9 ± 1.2 Ma for the lower line with an initial $^{40}Ar/^{36}Ar$ of 310 ± 44. The isochron age of each line is within the uncertainty of the mean age of the samples that define the isochron, and the uncertainties of the intercept values of both isochrons clearly include the value of the atmospheric $^{40}Ar/^{36}Ar$ ratio; each of these facts supports the assumption that the ages are geologically meaningful.

Because of the volcanic origin of bentonite units some of the authigenic clay-type minerals, especially the I/S mixed-layers such as those studied here, contain small and variable amounts of NH_4, which substitutes for K^+ in the interlayer sites (e.g., Nadeau and Bain 1986). However, such substitution does not affect the K-Ar age of the separated I/S, which strictly and only depends on the K/radiogenic ^{40}Ar ratio of the separated mineral particles, as has been shown in a dedicated K-Ar dating study of NH_4-illite rich I/S (Clauer et al. 2010).

DISCUSSION

Depending on the mechanism of illitization, one may expect different isotopic ages for nanometric illite crystals as they theoretically grow thicker and larger with time. The crystal growth theory of Eberl et al. (1998b) predicts that the growth rate is proportional to crystal size, indicating that the isotopic ages of the coarser fractions may be younger than those of the finer fractions, because the coarser crystals add new material at a faster rate than the finer crystals. This assumption was confirmed by the first K-Ar ages of bentonite beds from the East-Slovak Basin but not in the nearby Zempleni Mountains where illite

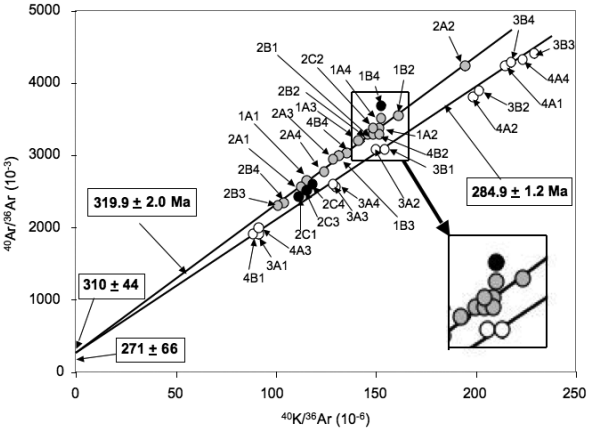

FIGURE 8. $^{40}Ar/^{36}Ar$ vs. $^{40}K/^{36}Ar$ isochron diagram of the different studied nanometric size fractions. The gray symbols define the upper isochron, the open ones the lower isochron and the black ones fall off the two lines, either in between or above the upper line.

crystallized from hot hydrothermal fluids (Clauer et al. 1997). Illitization of nanometric clays sampled from drill-holes of the basin lasted for several millions of years, whereas the various size fractions of the hydrothermal Zempleni clays provided a single age within analytical uncertainty. The duration of illitization depends on the driving parameters, and one can imagine two end-member histories: (1) a slow process accompanied by progressive temperature increase during burial, and (2) a rapid process with an essentially instantaneous temperature increase during a hydrothermal overprint. Such varied processes were reported in several studies (e.g., Clauer et al. 1997, 2013; Środoń and Clauer 2001; Honty et al. 2004; Środoń et al. 2006). Because we found homogeneous ages for the nanometric fractions of any given sample, as well as homogeneous mineral compositions, crystallite thickness distributions and reaction mechanisms, we are inclined to believe that the illitization of our samples occurred under abnormal episodic thermal conditions that provided narrow (i.e., within analytical uncertainty) ages of the different nanometric particles, as opposed to ages ranging beyond analytical uncertainty when recording burial-induced diagenetic crystal growth (e.g., Clauer et al. 2013). Only in the case of sample 4B, the finest (<0.02 μm) fraction is slightly, at the analytical limit, younger than the two coarser (0.02–0.05 and 0.1–0.2 μm) fractions (Table 3), which suggests that two nucleation episodes occurred successively in this sample.

Geological meaning of the K-Ar ages

The individual K-Ar ages obtained for the different size fractions for each of our samples are slightly higher for the basal layers relative to the equivalent top-layer samples. This is the case for the samples 1A and 1B, and 2A, 2B, and 2C collected from T3 and T4 bentonite units near Dalton, Georgia, but the age difference remains within analytical uncertainty. It looks as if, although induced by temperature increase and migration of hydrothermal fluids from nearby tectonic activity, illitization lasted slightly longer at the basal parts of the bentonite units.

There is no correlation between the K-Ar ages and the geographic dispersion of the samples: the younger ages were obtained on the northern Trenton, the central Lafayette and the southern Dirtseller sites. The K-Ar ages of illite-type nanometric particles from K-bentonite samples collected in Georgia and Alabama point to the occurrence of two hydrothermal overprints induced by nearby tectonic activity at 319.9 ± 2.0 and 284.9 ± 1.2 Ma. An additional pulse could have happened in between at 293 ± 2 Ma, but this needs to be confirmed. These K-Ar ages fit in the trends published previously on similar illite-smectite mixed layers from similar bentonite beds with regional age patterns between 240 and 270 Ma in the southwestern zone, between 270 and 300 Ma in the central zone and in the southern Appalachians, and from 315 to 370 Ma to the north (Elliott and Aronson 1987, 1993; Hay et al. 1988; Toulkeridis et al. 1998). The lower K-Ar age of the finest (<0.02 μm) fraction of sample 4B relative to the two coarser suggests a two-step crystallization, but the $\delta^{18}O$ values of this slightly younger fraction is not that of all the other younger nanometric fractions: <17.0 relative to >20.5‰. This difference in the $\delta^{18}O$ rather points rather to the analytical uncertainty on the K-Ar ages than to episodic nucleation and growth.

Restored into the regional structural evolution, both the previously published ages and those released here correlate well with the general understanding of the Late Paleozoic tectonic history of the southern Appalachians. The hinterland is partially composed of a complex mosaic of terranes that were amalgamated to the Laurentian margin during multiple phases of collision and related magmatism throughout Paleozoic time (Beaumont et al. 1987; Hatcher 2002). The culminating orogenic event of the Appalachians is the Late Mississippian-Pennsylvanian Alleghanian episode that involved an oblique, transpressive, and rotational collision between parts of Gondwana and previously accreted peri-Gondwanan assemblages, causing the formation of the Pangean supercontinent (Hatcher et al. 1989). In the central and southern Appalachians, the Alleghenian orogeny involved: (1) accretion of the Archean Suwannee terrane to the southeast margin of Laurentia (Horton et al. 1989); (2) lateral translation of previously accreted terranes along dextral strike-slip faults (Hatcher 2002); (3) a 300–325 Ma subduction-related magmatism and greenschist to amphibolite facies regional metamorphism of hinterland terranes (Hatcher et al. 1989; Hatcher 2005); and (4) development of a foreland fold-thrust belt that propagated into sedimentary rocks from the allochthonous pre-Alleghenian metamorphic rocks in the southern and central Appalachians (Hatcher et al. 1989). The final stage of the Alleghenian scenario involved head-on collision of southeastern Laurentia with Gondwana (Horton et al. 1989). The major product of head-on collision is the Blue Ridge-Piedmont megathrust sheet that transported crust amalgamated during all previous Paleozoic events at least 350 km onto the North American platform. The collision was finished about 265 Ma, forming supercontinent Pangaea and completing the Paleozoic Wilson Cycle of opening and closing of oceans.

Significance of the $\delta^{18}O$ values

The $\delta^{18}O$ values of the nanometric-to-micrometric subfractions of the different samples are internally very consistent. Interestingly, the fluid temperature and $\delta^{18}O$ composition can therefore likely be considered to be constant throughout the different bentonite beds known for their very low porosity and permeability. This could mean that illitization occurred when the bentonites were still somehow porous, consisting of volcanic glass in contact with locally isotopically homogeneous fluids.

Previous studies of authigenic feldspar fluid-inclusion microthermometric determinations from the same geographic area indicate a temperature range of 100–200 °C and a salinity of 18–21% NaCl equivalent for the interacting brines (Hearn et al. 1987; Elliott and Haynes 2002). Paleotemperatures well above 100 °C were also evidenced by completely reset apatite fission tracks and partially reset zircon fission tracks (Roden et al. 1993). Inserting the reference temperatures of 100 to 200 °C, which relate to the tectonic activity described in this region (Smith 2006), together with the $\delta^{18}O$ of 16 to 18‰ and of 20 to 22‰ for the two generations of illite, into the illite-water equilibrium oxygen isotope fractionation equation (Sheppard and Gilg 1996)

$$1000 \ln a^{18}_{\text{illite-water}} = 2.39\ 10^{6} T^{-2} - 4.19$$

gives $\delta^{18}O$ of about 4 ± 1‰ for the fluids at 100 °C in the Dalton district and of about 8 ± 1‰ in the Lafayette, Trenton, and

Distseller districts. The $\delta^{18}O$ values of the same fluids would be 11 ± 1 and 15 ± 1‰ in the two districts, respectively, at a temperature of 200 °C. Assuming that illite precipitated at isotopic equilibrium, the $\delta^{18}O$ of the parental fluids did not change during local crystal growth, as the $\delta^{18}O$ values are systematically very homogeneous (range of 0.1 to 0.9‰ for the extreme $\delta^{18}O$ values for each set of analyzed size fractions), but it expectedly changed with the geographic location of the samples and the timing of illitization. Further useful discussion would require better constrained temperature estimates, which might allow a deeper insight as to how the chemical and isotopic characteristics of the fluids parental to the illite varied in time and space. What is clear, however, is that the high-$\delta^{18}O$ values calculated from the measured illite $\delta^{18}O$ compositions and the assumed temperatures strongly suggest isotope exchange at elevated temperature in a rock-dominated system.

The significantly higher $\delta^{18}O$ values of the illite crystals from the Lafayette, Trenton, and Dirtseller districts that precipitated later at about 285 Ma, suggest that the crystallization temperature was lower (Figs. 9a and 9b). An alternative suggestion is that the water $\delta^{18}O$ was higher during the more recent tectonic activity due to more pervasive water-rock interaction in a rock-dominated system (e.g., Aagard and Egeberg 1998), unless both a lower crystallization temperature and a higher fluid $\delta^{18}O$ were combined.

Information from δD values

As discussed previously, the δD values of the different size fractions do not give a consistent pattern, as was also found for illite-enriched nanometric particles from bentonite units of the East Slovak Basin (Clauer et al. 2013). Therefore, the δD results do not support a systematic occurrence of agglomerated nanometric particles in the different size fractions, because there is no consistent evidence of δD being the same from fine to coarse particles within a given sample, and additionally $\delta^{18}O$ does not change as significantly as δD (Fig. 9). Other factors having a significant impact on the illite δD values could have varied, depending for instance on the immediate environment of the nucleating and growing crystals, and also on potential exchange with ground waters since crystallization (Longstaffe and Ayalon 1990).

Variable initial $\delta^{18}O$-δD composition of the hydrothermal fluids resulting from a long-lived illitization process is not a viable model here, because illitization is considered to be almost instantaneous in the present case. The $\delta^{18}O$ of the fluids appears then to depend on geographic location and crystallization timing with probable varied thermal gradients, changing water/rock interactions, or on other processes not yet identified. Beyond these aspects, differences in the nucleation and growth processes may induce changes in δD, and therefore could result in changing $^{18}O/^{16}O$ and D/H of the hydroxyl groups because of interaction with changing fluids during particle growth. While the capacity for isotope resetting during post-precipitation processes is still debated, it is clear that D/H is more susceptible to such changes than $^{18}O/^{16}O$ (e.g., Bird and Chivas 1988; Longstaffe and Ayalon 1990, and references therein).

The extremely constant $\delta^{18}O$ values of the different nanometric illite fractions represents a strong argument against changing

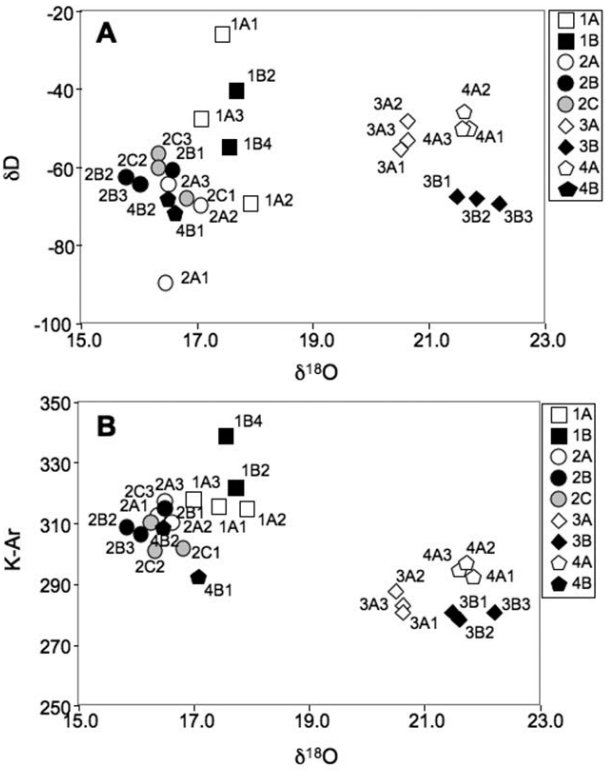

FIGURE 9. $\delta^{18}O$ vs. δD (**a**) and $\delta^{18}O$ vs. K-Ar (**b**) plots for the different studied nanometric size fractions.

fluids during the nucleation and growth processes, and also against post-precipitation changes of the hydroxyls, as about half of the illite oxygen is present as hydroxyls in the mineral structure. Bechtel and Hoernes (1990) estimated that isotope fractionation between framework and hydroxyl oxygen in illite is about 15‰ at 200 °C, and even higher at lower temperature, so constant mineral $\delta^{18}O$ implies little post-precipitation exchange of hydroxyl oxygen. Clearly, except if proton exchange allowing H isotopic composition of hydroxyls to change without affecting the O isotopic composition, such intra-mineral considerations do not influence D/H and so cannot explain the δD scatter obtained here. Until such a proton-exchange hypothesis is tested, we decided to report, although without a satisfactory explanation, to contribute to the still limited analytical database. Initial smectite layers may also preserve interlayer water of an isotopic composition acquired from the environment prior to illitization. However, the specific sample preparation with PVP polymer and the infinite osmotic dispersion cleans the smectite interlayers of the crystals by removing the cations and could, perhaps, alter the structural hydroxyl D/H. This would imply hydrogen isotope exchange at low temperature over a very short hourly timescale, which of course needs also to be checked specifically.

IMPLICATIONS

Our newly determined K-Ar ages on K-bentonite samples from northwest Georgia correlate well with the general understanding of the Late Paleozoic tectonic history of the southern

Appalachians. The culminating orogenic event is the Late Mississippian-Pennsylvanian episode that involved an oblique, transpressive, and rotational collision between parts of Gondwana and previously accreted peri-Gondwanan assemblages. In the central and southern Appalachians, the Alleghenian orogeny involved also the development of a foreland fold-thrust belt that propagated into sedimentary rocks from the allochthonous pre-Alleghenian metamorphic rocks in the southern and central Appalachians that ended about 265 Ma ago.

The two generations of illite crystals yield extremely constant $\delta^{18}O$ values at 17 ± 1‰ for the older and at 21 ± 1‰ for the younger. If crystallization temperatures of the nanometric illite were between 100 and 200 °C, as suggested by microthermometric measurements, the interacting fluids were of hydrothermal origin with $\delta^{18}O$ values of 4 ± 1‰ in the Dalton district and of 8 ± 1‰ in the Lafayette, Trenton, and Dirtseller districts at an implied temperature of 100 °C, and of 11 ± 1 and 15 ± 1‰, respectively, in the same locations at an implied temperature of 200 °C. If illite precipitated at isotopic equilibrium, the $\delta^{18}O$ of the fluids remained unchanged during local crystal growth, but varied depending on the geographic location of the samples and timing of illitization. The δD values are widely scattered from –70 to –45‰ (V-SMOW) for most size fractions.

The combined mineralogical XRD study applied to nanometric illite-type crystals to assess their crystal thickness distributions, together $\delta^{18}O$ and δD isotopic determinations, provides further insights into illitization such as controlled constant ages, constant clay mineralogy, constant crystallite size distributions for all of the nucleating and growing illite-type crystals of each sample, constant $\delta^{18}O$ values implying constant fluids. All these parameters point to geologically sudden crystallization episodes that support episodic tectono-thermal activity. Complementary K-Ar dating shows that the samples from different locations reacted at different times, with only one sample deviating from concomitant nucleation and growth process. However, the restricted number of samples makes it difficult to enlarge the picture to a regional scale including the search for migration of heat sources and associated fluid flows, as well as timing of their occurrence(s).

Acknowledgments

We are deeply indebted to the two reviewers F.J. Longstaffe and D. Awwiller for their very thoughtful and constructive comments that helped improve and focus the previous draft of this note. We are also thankful to the editorial board, especially to Associate Editor H. Xu for very efficient handling of the review round. We also extend sincere thanks to Sam Chaudhuri for having organized the sampling together with Tim Chowns, S. Holland, and P. Schroeder, to Jan Środoń for separation of the nanometric size fractions at the Geological Institute PAN of Krakow, Poland, and to Robert Wendling, Raymond Wendling, Daniel Tisserant, and Raymond Winkler of the Centre de Géochimie de la Surface (CNRS/ULP) for technical assistance during the study. SUERC was supported by NERC and a consortium of Scottish Universities.

References cited

Aagard, P., and Egeberg, P.K. (1998) Formation waters and diagenetic modifications: General trends exhibited by oil fields from the Norwegian shelf—A model for formation waters in oil prove subsiding basins. In G.B. Arehard and J.R. Hulsten, Eds., Water-Rock Interaction WRI-9, 281–284. Balkema, Rotterdam.

Altaner, S.P., and Ylagan, R.F. (1997) Comparison of structural models of mixed-layer illite/smectite and reaction mechanisms of smectite illitization. Clays and Clay Minerals, 45, 517–533.

Beaumont, C., Quinland, G.M., and Hamilton, J. (1987) The Alleghanian orogeny and its relationship to the evolution of the Eastern Interior, North America. In C. Beaumont and A.J. Tankard, Eds., Sedimentary Basins and Basin-Forming Mechanisms. Canadian Society of Petroleum Geologists Memoir, 12, 425–445.

Bechtel, A., and Hoernes, S. (1990) Oxygen isotope fractionation between oxygen of different sites in illite minerals: A potential single-mineral thermometer. Contributions to Mineralogy and Petrology, 104, 463–470.

Bethke, C.M. (1986) Hydrologic constraints on the genesis of the Upper Mississippi Valley mineral district from Illinois basin brines. Economic Geology, 81, 233–249.

Bethke, C.M., and Marshak, S. (1990) Brine migrations across North America—The plate tectonics of groundwater. Annual Review of Earth and Planetary Sciences, 18, 287–315.

Bigeleisen, J., Perlman, M.L., and Prosser, H.C. (1952) Conversion of hydrogenic materials to hydrogen for isotopic analysis. Analytical Chemistry, 24, 356–1357.

Bird, M.I., and Chivas, A.R. (1988) Stable-isotope evidence for low temperature kaolinitic weathering and post-formational hydrogen-isotope exchange in Permian kaolinites. Chemical Geology (Isotope Geosciences), 72, 249–265.

Bonhomme, M., Thuizat, R., Pinault, Y., Clauer, N., Wendling, A., and Winkler, R. (1975) Méthode de datation potassium-argon appareillage et technique. In Notes Techniques de l'Institut de Géologie, Université Louis Pasteur, Strasbourg, 3, 53 p.

Borthwick, J., and Harmon, R.S. (1982) A note regarding ClF_3 as an alternative to BrF_5 for oxygen isotope analysis. Geochimica et Cosmochimica Acta, 46, 1665–1668.

Bove, D.J., Eberl, D.D., McCarty, D.K., and Meeker, G.P. (2002) Characterization of modeling of illite crystal particles and growth mechanisms in a zoned hydrothermal deposit, Lake City, Colorado. American Mineralogist, 87, 1546–1556.

Carter, B.D., and Chowns, T.M. (1989) Stratigraphic and environmental relationships of Middle and Upper Ordovician rocks in Northwest Georgia and Northeast Alabama. In B.D. Keith, Ed., The Trenton Group (Upper Ordovician Series) of Eastern North America, Deposition, Diagenesis, Petroleum, 29, 17–26. Studies in Geology, American Association of Petroleum Geologists, Tulsa, Oklahoma.

Chen, Z., Riciputi, L.R., Mora, C.I., and Fishman, N.S. (2001) Regional fluid migration in the Illinois basin: evidence from in situ oxygen isotope analysis of authigenic K-feldspar and quartz from the Mount Simon Sandstone. Geology, 29, 1067–1070.

Clauer, N., Środoń, J., Francu, J., and Šucha, V. (1997) K-Ar dating of illite fundamental particles separated from illite-smectite. Clay Minerals, 32, 181–196.

Clauer, N., Liewig, N., and Bobos, I. (2010) K-Ar, $\delta^{18}O$ and REE constraints on the genesis of ammonium illite from the Harghita Bai hydrothermal system, Romania. Clay Minerals, 45, 393–411.

Clauer, N., Honty, M., Fallick, A.E., and Šucha, V. (2013) Regional illitization in bentonite beds from East Slovak Basin based on isotopic characteristics (K-Ar, $\delta^{18}O$ and δD) of illite-type nanoparticles. Clay Minerals, in press.

Clayton, R.N., and Mayeda, T.K. (1963) The use of bromine pentafluoride in the extraction of oxygen from oxides and silicates for isotopic analysis. Geochimica et Cosmochimica Acta, 27, 43–52.

Donnelly, T., Waldron, S., Tait, A., Dougans, J., and Bearhop, S. (2000) Hydrogen isotope analysis of natural abundance and deuterium-enriched waters by reduction over chromium on-line to a dynamic dual inlet isotope-ratio mass spectrometer. Rapid Communications in Mass Spectrometry, 15, 1297–1303.

Dozy, J.J. (1970) A geological model for the genesis of the lead-zinc ores of the Mississippi Valley, U.S.A. Transactions Institution Mining and Metallogeny, Section B, 79, 163–170.

Drahovzal, J.A., and Neathery, T.L. (1971) The middle and upper Ordovician stratigraphy of the Alabama Appalachians, In J.A. Drahovzal and T.L. Neathery, Eds., The middle and upper Ordovician stratigraphy of the Alabama Appalachians, 1–62. Guidebook for the Ninth Annual Fieldtrip, Alabama Geological Society, Tuscaloosa.

——— (1985) Lithostratigraphy of Upper Ordovician strata in Alabama. Alabama Geological Survey Circular, 124, 55 p.

Drits, V.A., Eberl, D.D., and Środoń, J. (1998) XRD measurement of mean thickness, thickness ditribution and strain for illite and illite/smectite crystallites by the Bertaut-Warren-Averbach technique. Clays and Clay Minerals, 46, 461–475.

Dudek, T., and Środoń, J. (1996) Identification of illite/smectite by X-ray powder diffraction taking into account the lognormal distribution of crystal thickness. Geologica Carpathica, 5, 21–32.

Duffin, M.E., Lee, M., de V. Klein, G., and Hay, R.L. (1989) Potassic diagenesis of Cambrian sandstones and Precambrian granitic basement in UPH-3 deep hole, Upper Mississippi Valley, U.S.A. Journal of Sedimentary Petrology, 59, 848–861.

Eberl, D.D., and Środoń, J. (1988) Ostwald ripening and interparticle-diffraction effects from illite crystals. American Mineralogist, 73, 1335–1345.

Eberl, D.D., Drits, V., Środoń, J., and Nüesch, R. (1996) MudMaster: a program for calculating crystallite size distribution and strain from the shapes of X-ray diffraction peaks. U.S. Geological Survey, Open-File Report, 96-171.

Eberl, D.D., Nüesch, R., Šucha, V., and Tsipursky, S. (1998a) Measurement of fundamental illite particle thickness by X-ray diffraction using PVP-10 intercalation. Clays and Clay Minerals, 46, 89–97.

Eberl, D.D., Drits, V.A., and Środoń, J. (1998b) Deducing growth mechanisms

for minerals from the shapes of crystal size distributions. American Journal of Sciences, 298, 499–533.
——— (2001) User's guide to GALOPER—a program for simulating the shapes of crystal size distributions – and associated programs. U.S. Geological Survey, Open-File Report, OF00-505, 44 p.
Eberl, D.D., Blum, A.E., and Serravezza, M. (2011) Anatomy of a metabentonite: Nucleation and growth of illite crystals and their coalescence into mixed-layer illite/smectite. American Mineralogist, 96, 586–595.
Elliott, W.C., and Aronson, J.L. (1987) Alleghanian episode of K-bentonite illitization in the southern Appalachian Basin. Geology, 15, 735–739.
——— (1993) The timing and extent of illite formation in Ordovician K-bentonites at the Cincinnati Arch, the Nashville Dome and north-eastern Illinois basin. Basin Research, 5, 125–135.
Elliott, W.C., and Haynes, J.T. (2002) The chemical character of fluids forming diagenetic illite in the Southern Appalachian Basin. American Mineralogist, 87, 1519–1527.
Fallick, A.E., Macaulay, C.I., and Haszeldine, R.S. (1993) Implications of linearly correlated oxygen and hydrogen isotopic compositions for kaolinite and illite in the Magnus Sandstone, North Sea. Clays and Clay Minerals, 41, 184–190.
Fishman, N.S. (1997) Basin-wide fluid movement in a Cambrian paleoaquifer: Evidence from the Mt. Simon Sandstone, Illinois and Indiana. In I.P. Montañez, J.M. Gregg, and K.L. Shelton, Eds., Basin-wide diagenetic patterns: Integrated petrologic, geochemical, and hydrologic considerations, 57, 221–234. Special Publication, Society of Economic Paleontologists and Mineralogists, Tulsa, Oklahoma.
Garven, G., and Freeze, R.A. (1984) Theoretical analysis of the role of groundwater flow in the genesis of stratabound ore deposits. 1. Mathematical and numerical model and 2. Quantitative results. American Journal of Science, 284, 1085–1174.
Girard, J.P., and Barnes, D.A. (1995) Illitization and paleothermal regimes in the Middle Ordovician St. Peter Sandstone, central Michigan basin: K-Ar, oxygen isotope, and fluid inclusion data. American Association of Petroleum Geologists Bulletin, 79, 49–69.
Grathoff, G.H., Moore, M.M., Hay, R.L., and Wemmer, K. (2001) Origin of illite in the lower Paleozoic of the Illinois basin: evidence for brine migrations. Geological Society of America Bulletin, 113, 1092–1104.
Harper, D.A., Longstaffe, F.J., Wadleigh, M.A., and McNutt, R.H. (1995) Secondary K-feldspar at the Precambrian-Paleozoic unconformity, southwestern Ontario. Canadian Journal of Earth Sciences, 32, 1432–1450.
Hatcher, R.D. Jr. (2002) Alleghanian (Appalachian) orogeny, a product of zipper tectonics: Rotational transpressive continent-continent collision and closing of ancient oceans along irregular margins. In J.R. Martínez Catalán, R.D. Hatcher Jr., R. Arenas, and F. Díaz García, Eds., Variscan-Appalachian Dynamics: The building of the late Paleozoic basement. Geological Society of America Special Paper, 364, Boulder, Colorado, 199–208.
——— (2005) Regional geology of North America—Southern and Central Appalachians. Encyclopedia of Geology, Elsevier, London, 72–81.
Hatcher, R.D. Jr., Thomas, W.A., Geiser, P.A., Snoke, A.W., Mosher, S., and Wiltschko, D.V. (1989) Alleghanian Orogen. In R.D. Hatcher Jr., W.A. Thomas, and G.W. Viele, Eds., The Appalachian-Ouachita orogen in the United States, vol. F-2, p. 233–318. Geology of North America, Geological Society of America, Boulder, Colorado.
Hay, R.L., Lee, M., Kolata, D.R., Matthews, J.C., and Morton, J.P. (1988) Episodic potassic diagenesis of Ordovician tuffs in the Mississippi Valley area. Geology, 16, 743–747.
Hearn, P.P. Jr., and Sutter, J.F. (1985) Authigenic potassium feldspar in Cambrian carbonates: Evidence of Alleghanian brine migration. Science, 228, 1529–1531.
Hearn, P.P. Jr., Sutter, J.F., and Belkin, H.E. (1987) Evidence for Late-Paleozoic brine migration in Cambrian carbonate rocks of the central and southern Appalachians: Implications for Mississippi Valley-type sulfide mineralization. Geochimica et Cosmochimica Acta, 51, 1323–1334.
Honty, M., Uhlík, P., Sucha, V., Caplovicová, M., Francù, J., Clauer, N., and Biron, A. (2004) Smectite-to-illite alteration in salt-bearing bentonites (the East Slovak Basin). Clays and Clay Minerals, 52, 533–551.
Horton, J.W. Jr., Drake, A.A., and Rankin, D.W. (1989) Tectonostratigraphic terranes and their Paleozoic boundaries in the Central and Southern Appalachians. In R.D. Dallmeyer, Ed., Terranes in the Circum-Atlantic Paleozoic Orogens. Geological Society of America Special Paper, 230, 213–245.
Huff, W.D., and Kolata, D.R. (1990) Correlation of the Ordovician Deicke and Millbrig K-bentonites between the Mississippi Valley and the southern Appalachians. American Association of Petroleum Geologists Bulletin, 74, 1736–1747.
Huff, W.D., Bergstrom, S.M., and Kolata, D.R. (1986) Gigantic Ordovician ash fall in North America and Europe: Biological, tectonomagmatic, and event-stratigraphic significance. Geology, 20, 875–878.
Jackson, M.L. (1975) Soil Chemical Analysis—advanced course, 386 p. Self-published, Madison, Wisconsin.
Kolata, D.R., Huff, W.D., and Bergström, S.M. (1996) Ordovician K-bentonites of eastern North America. Geological Society of America, Special Paper, 313, 1–84.
Leslie, S.A., Bergström, S.M., and Huff, W.D. (2008) Ordovician K-bentonites discovered in Oklahoma. Oklahoma Geology Notes, 68, 4–14.
Liu, J., Hay, R.L., Deino, A., and Kyser, T.K. (2003) Age and origin of authigenic K-feldspar in uppermost Precambrian rocks in the North American Midcontinent. Geological Society of America Bulletin, 115, 422–433.
Longstaffe, F.J., and Ayalon, A. (1990) Hydrogen-isotope geochemistry of diagenetic clay minerals from Cretaceous sandstones, Alberta, Canada: Evidence for exchange. Applied Geochemistry, 5, 657–668.
Macaulay, C.I., Fallick, A.E., Haszeldine, R.S., and, Graham, C.M. (2000) Methods of laser-based stable isotope measurement applied to diagenetic cements and hydrocarbon reservoir quality. Clay Minerals, 35, 317–326.
Marshall, B.D., Woodard, H.H., and DePaolo, D.J. (1986) K-Ca-Ar systematics of authigenic sanidine from Waukau, Wisconsin, and the diffusivity of argon. Geology, 14, 936–938.
Moore, D.M., and Reynolds, R.C. Jr. (1997) X-ray Diffraction and the Identification and Analysis of Clay Minerals, 378 p. Oxford University Press, 2nd ed. New York.
Nadeau, P.H., and Bain, D.C. (1986) Composition of some smectites and diagenetic illitic clays and implications for their origin. Clays and Clay Minerals, 34, 455–464.
Nadeau, P.H., Wilson, M.J., McHardy, W.J., and Tait, J.M. (1984) Interstratified clays as fundamental particles. Science, 225, 923–925.
Nier, A.O. (1950) A redetermination of the relative abundances of the isotopes of carbon, nitrogen, oxygen, argon and potassium. Physical Review, 77, 789–793.
Odin, G.S., and others. (1982) Interlaboratory standards for dating purposes. In G.S. Odin, Ed., Numerical Dating in Stratigraphy, 123–148. Wiley, Chichester.
Oliver, J. (1986) Fluids expelled tectonically from orogenic belts: Their role in hydrocarbon migration and other geologic phenomena. Geology, 14, 99–102.
Raymond, D.E., Osborne, W.E., Copeland, C.W., and Neathery, T.L. (1988) Alabama stratigraphy. Alabama Geological Survey Circular, 140, 97p.
Roden, M.K., Elliott, W.C., Aronson, J.L., and Miller, D.S. (1993) Comparison of fission-track ages of apatite and zircon to the K/Ar ages of illite-smectite (I/S) from Ordovician K-bentonites, southern Appalachian basin. Journal of Geology, 101, 633–641.
Sheppard, S.M.F., and Gilg, H.A. (1996) Stable isotope geochemistry of clay minerals. Clay Minerals, 31, 1–24.
Smith, L.B. Jr. (2006) Origin and Reservoir Characteristics of Upper Ordovician Trenton-Black River Hydrothermal Dolomite Reservoirs in New York. American Association of Petroleum Geologists Bulletin, 90, 1691–1718.
Środoń, J., and Clauer, N. (2001) Diagenetic history of Lower Palaeozoic sediments in Pomerania (northern Poland) traced across the Teisseyre-Tornquist tectonic zone using mixed-layer illite-smectite. Clay Minerals, 36, 15–27.
Środoń, J., Elsass, F., McHardy, W.J., and Morgan, D.J. (1992) Chemistry of illite/smectite inferred from TEM measurements of fundamental particles. Clay Minerals, 27, 137–158.
Środoń, J., Clauer, N., Banas, M., and Wojtowicz, A. (2006) K-Ar evidence for a Mesozoic thermal event superimposed on burial diagenesis of the Upper Silesia Coal Basin. Clay Minerals, 41, 669–690.
Stamatakos, J., Hirt, A.M., and Lowrie, W. (1996) The age and timing of folding in the central Appalachians from paleomagnetic results. Geological Society of America Bulletin, 108, 815–829.
Steiger, R.H., and Jäger, E. (1977) Subcommission on Geochronology: Convention on the use of decay constants in geochronology and cosmochronology. Earth and Planetary Science Letters, 36, 359–362.
Szabo, M.W., Osborne, W.E., Copeland, C.W. Jr., and Neathery, T.L. (1988) Geologic map of Alabama. Alabama Geological Survey, Special Map 220, scale 1:250000.
Toulkeridis, T., Clauer, N., Chaudhuri, S., and Goldstein, S.L. (1998) Multi-method (K-Ar, Rb-Sr, Sm-Nd) dating of bentonite minerals from eastern United States. Basin Research, 10, 261–270.
Woodard, H.H. (1972) Syngenetic sanidine beds from Middle Ordovician Saint Peter Sandstone, Wisconsin. Journal of Geology, 80, 323–332.
Ziegler, K., and Longstaffe, F.J. (2000a) Multiple episodes of clay alteration at the Precambrian/Paleozoic unconformity, Appalachian basin: isotopic evidence for long-distance and local fluid migrations. Clays and Clay Minerals, 48, 474–493.
——— (2000b) Clay mineral authigenesis along a mid-continental scale fluid conduit in Palaeozoic sedimentary rocks from southern Ontario, Canada. Clay Minerals, 35, 239–260.

Manuscript received February 20, 2013
Manuscript accepted July 2, 2013
Manuscript handled by Hongwu Xu